16th World Congress in Computational Mechanics (WCCM)
21-26 July 2024, Vancouver, Canada
A. Korobenko, M. Laforest, S. Prudhomme, R. Vaziri (Eds)

A NEW CONCEPT FOR EMBEDDING SUB-STRUCTURES VIA LEVEL-SETS

T.P. Fries[1,2], J. Neumeyer[1,3] and M.W. Kaiser[1,4]

[1] Institute of Structural Analysis
Graz University of Technology
Lessingstr. 25, 8010 Graz, Austria
www.ifb.tugraz.at

[2]e-mail: fries@tugraz.at (corresponding author)

[3]e-mail: jonas.neumeyer@tugraz.at

[4]e-mail: michael.kaiser@tugraz.at

Key words: finite strain theory, fibres, membranes, sub-structures, fictitious domain method, PDEs on manifolds, implicit geometry, level-set method, anisotropy.

Abstract. A framework is presented to continuously embed sub-structures such as fibres and membranes into otherwise homogeneous, isotropic bulk materials. The bulk material is modeled with classical finite strain theory. The sub-structures are geometrically defined via all level sets of a scalar function over the bulk domain. A mechanical model that is simultaneously applicable to all level sets is given and coupled to the bulk material. This results in a new concept for anisotropic materials with possible applications in biological tissues, layered rocks, composites, and textiles. For the numerical analysis, the bulk domain is discretized possibly using higher-order finite elements which do not conform to the level sets implying the shapes of the embedded sub-structures. Numerical results confirm the success of the proposed embedded sub-structure models in different contexts.

1 Introduction

A new concept for including sub-structures such as fibres and membranes into bulk materials is proposed and generalized from [8, 10, 7]. The bulk domain is equipped with level-set functions [12] whose isosurfaces and/or isolines represent the geometries of the embedded sub-structures. Each level-set function represents an infinite set of continuously embedded, homogenized sub-structures. This enables a new concept for advanced, anisotropic materials such as biological tissues, layered rocks, composites, and textiles.

Mechanical models are proposed which consider the physics on the individual level sets including the generalization into the whole bulk domain [8, 10]. Previous works of the

authors focus on reformulating and generalizing classical models for explicit geometries to the implicit case, see [9] for ropes and membranes, and [13, 14, 16] for shells. The authors extend their models from the analysis of *single* geometries to the simultaneous analysis of *all* geometries as implied by all level sets within some bulk domain, see [8, 7, 10] for membranes and [11] for shells. Herein, the bulk models for the sub-structures are coupled to classical homogeneous and isotropic mechanical models resulting in a new class of models. For the numerical analysis, the bulk domain is meshed using classical, higher-order elements. It is noteworthy that these elements do not have to align to the embedded level sets which is otherwise characteristic for a fictitious domain method (FDM). However, the present approach does not come with the usual challenges of FDMs. That is, boundary conditions and numerical integration are done as in the classical FEM and there is no need for stabilization. The numerical approach for treating PDEs simultaneously on all level sets may be traced back to [1, 4, 3] in the context of transport applications and was called Bulk Trace FEM in [8].

In Section 2, the mechanical model of the homogeneous and isotropic bulk material is given, which is the classical boundary value problem (BVP) in finite strain theory. The mechanics of the embedded sub-structures is outlined in Section 3 following [8, 10]. The coupled models are presented in Section 4 in strong and weak form, enabling a tailored finite element analysis. Numerical results are given in Section 5: One test case considers a two-dimensional bulk domain with embedded *fibres*, the other a three-dimensional bulk domain with embedded *membranes*. The paper ends in Section 6 with a summary and conclusions.

2 Mechanical quantities in the bulk domain

In finite strain or large displacement theory, an undeformed, d-dimensional *material* domain $\Omega_{\boldsymbol{X}} \subset \mathbb{R}^d$ and a deformed *spatial* domain $\Omega_{\boldsymbol{x}}$ are distinguished and connected via the displacement field $\boldsymbol{u}(\boldsymbol{X}) : \mathbb{R}^d \to \mathbb{R}^d$ as

$$\Omega_{\boldsymbol{x}} = \{\boldsymbol{x} = \boldsymbol{X} + \boldsymbol{u}(\boldsymbol{X}), \boldsymbol{X} \in \Omega_{\boldsymbol{X}}\}.$$

As usual, we employ (mostly) capital letters with the material and lowercase letters with the spatial configuration, respectively. With the displacement field $\boldsymbol{u}(\boldsymbol{X})$ and $\boldsymbol{x} = \boldsymbol{X} + \boldsymbol{u}(\boldsymbol{X})$, the resulting *bulk deformation gradient* is

$$\mathbf{F}_\Omega = \nabla_{\boldsymbol{X}} \boldsymbol{x}(\boldsymbol{X}) = \mathbf{I} + \nabla_{\boldsymbol{X}} \boldsymbol{u}(\boldsymbol{X}),$$

where $\mathbf{I}$ is the $(d \times d)$-identity matrix. The following mechanical quantities result for a linear-elastic, homogeneous, and isotropic Saint Venant–Kirchhoff solid in the bulk

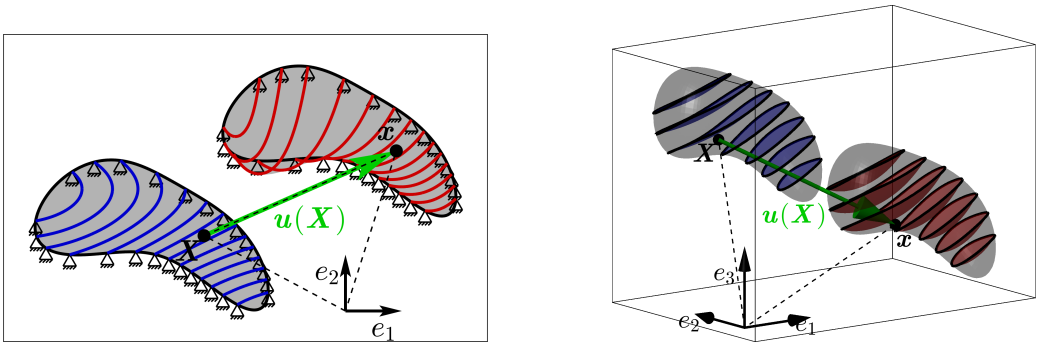

(a) situation in 2D (b) situation in 3D

Figure 1: Undeformed *material* configuration and deformed *spatial* configuration in two and three dimensions. The bulk domains $\Omega_{\boldsymbol{X}}$ and $\Omega_{\boldsymbol{x}}$ are shown in gray. The undeformed level sets $\Gamma^c_{\boldsymbol{X}}$ are blue and the deformed level sets $\Gamma^c_{\boldsymbol{x}}$ are red.

domain:

$$\begin{aligned}
\text{Green-Lagrange strain tensor in } \Omega_{\boldsymbol{X}}\text{:}\quad & \mathbf{E}_\Omega = {}^1\!/_2 \cdot \left(\mathbf{F}_\Omega^{\mathrm{T}} \cdot \mathbf{F}_\Omega - \mathbf{I}\right), \\
\text{second Piola-Kirchhoff stress tensor in } \Omega_{\boldsymbol{X}}\text{:}\quad & \mathbf{S}_\Omega = \lambda_\Omega \cdot \operatorname{trace}\left(\mathbf{E}_\Omega\right) + 2\mu_\Omega \mathbf{E}_\Omega, \\
\text{Cauchy stress tensor in } \Omega_{\boldsymbol{x}}\text{:}\quad & \boldsymbol{\sigma}_\Omega = \frac{1}{\det \mathbf{F}_\Omega} \cdot \mathbf{F}_\Omega \cdot \mathbf{S}_\Omega \cdot \mathbf{F}_\Omega^{\mathrm{T}}, \\
\text{first Piola-Kirchhoff stress tensor:}\quad & \mathbf{K}_\Omega = \mathbf{F}_\Omega \cdot \mathbf{S}_\Omega
\end{aligned}$$

where the two Lamé constants in the bulk domain are defined as $\lambda_\Omega = \frac{E \cdot \nu}{(1+\nu)\cdot(1-2\nu)}$, $\mu_\Omega = \frac{E}{2(1+\nu)}$, with Young's modulus E and Poisson's ratio ν of the bulk material.

3 Mechanical quantities of the embedded sub-structures

Let there be a level-set function $\phi\left(\boldsymbol{X}\right) \in \Omega_{\boldsymbol{X}}$ whose level sets define continuously embedded sub-structures $\Gamma^c_{\boldsymbol{X}}$ in the material domain and $\Gamma^c_{\boldsymbol{x}}$ in the deformed domain, see Fig. 1:

$$\Gamma^c_{\boldsymbol{X}} = \left\{\boldsymbol{X} \in \Omega_{\boldsymbol{X}} : \phi(\boldsymbol{X}) = c\right\}, c \in \left(\phi^{\min}, \phi^{\max}\right), \tag{1}$$

$$\Gamma^c_{\boldsymbol{x}} = \left\{\boldsymbol{x} \in \Omega_{\boldsymbol{x}} : \phi(\boldsymbol{x}) = c\right\}, c \in \left(\phi^{\min}, \phi^{\max}\right), \tag{2}$$

where $\phi^{\min} = \inf_{\boldsymbol{X}\in\Omega_{\boldsymbol{X}}} \phi\left(\boldsymbol{X}\right)$ and $\phi^{\max} = \sup_{\boldsymbol{X}\in\Omega_{\boldsymbol{X}}} \phi\left(\boldsymbol{X}\right)$. For two-dimensional bulk domains, $d = 2$, this is a set of fibres (ropes, cables), and in three dimensions, $d = 3$, this is a set of embedded membranes. It is noted, that also in three dimensions, fibres may be embedded using *two* level-set functions per fibre-family, however, this is not considered herein. Based on the level sets, we may easily compute normal vectors in the undeformed

and deformed configurations as

$$\boldsymbol{N}(\boldsymbol{X}) = \frac{\boldsymbol{N}^\star}{\|\boldsymbol{N}^\star\|} \quad \text{with} \quad \boldsymbol{N}^\star = \nabla_{\boldsymbol{X}}\phi\left(\boldsymbol{X}\right),\ \boldsymbol{X} \in \Omega_{\boldsymbol{X}},$$
$$\boldsymbol{n}(\boldsymbol{x}) = \frac{\boldsymbol{n}^\star}{\|\boldsymbol{n}^\star\|} \quad \text{with} \quad \boldsymbol{n}^\star = \nabla_{\boldsymbol{x}}\phi\left(\boldsymbol{x}\right),\ \boldsymbol{x} \in \Omega_{\boldsymbol{x}}.$$

The projector fields $\mathbf{P}\left(\boldsymbol{X}\right) = \mathbf{I} - \boldsymbol{N} \otimes \boldsymbol{N}$ in $\Omega_{\boldsymbol{X}}$ and $\mathbf{p}\left(\boldsymbol{x}\right) = \mathbf{I} - \boldsymbol{n} \otimes \boldsymbol{n}$ in $\Omega_{\boldsymbol{x}}$ are readily computed.

3.1 Differential operators

It is important to distinguish (classical) differential operators acting in the bulk space from those acting on the level sets which may be called *tangential* or *surface* operators. Here, these operators are defined with respect to the undeformed configuration but extend straightforwardly to the deformed situation as well. The *surface gradient* of a scalar function $f(\boldsymbol{X}) : \Omega_{\boldsymbol{X}} \to \mathbb{R}$ results as [2, 5, 15]

$$\nabla^{\Gamma}_{\boldsymbol{X}} f = \mathbf{P} \cdot \nabla_{\boldsymbol{X}} f, \tag{3}$$

where $\nabla_{\boldsymbol{X}} f$ is the classical gradient in the undeformed d-dimensional bulk domain. For the directional and covariant surface gradients of some *vector* function $\boldsymbol{u}\left(\boldsymbol{X}\right) : \Omega_{\boldsymbol{X}} \to \mathbb{R}^d$, one obtains

$$\nabla^{\Gamma,\mathrm{dir}}_{\boldsymbol{X}} \boldsymbol{u} = \nabla_{\boldsymbol{X}} \boldsymbol{u} \cdot \mathbf{P}, \qquad \nabla^{\Gamma,\mathrm{cov}}_{\boldsymbol{X}} \boldsymbol{u} = \mathbf{P} \cdot \nabla_{\boldsymbol{X}} \boldsymbol{u} \cdot \mathbf{P},$$

respectively. Concerning the *surface divergence* of vector functions $\boldsymbol{u}\left(\boldsymbol{X}\right)$ and tensor functions $\mathbf{A}(\boldsymbol{X}) : \Omega_{\boldsymbol{X}} \to \mathbb{R}^{d\times d}$, there holds

$$\mathrm{Div}_{\Gamma}\, \boldsymbol{u}\left(\boldsymbol{X}\right) = \mathrm{tr}\left(\nabla^{\Gamma,\mathrm{dir}}_{\boldsymbol{X}} \boldsymbol{u}\right) = \mathrm{tr}\left(\nabla^{\Gamma,\mathrm{cov}}_{\boldsymbol{X}} \boldsymbol{u}\right) =: \nabla^{\Gamma}_{\boldsymbol{X}} \cdot \boldsymbol{u}, \tag{4}$$

$$\mathrm{Div}_{\Gamma}\, \mathbf{A}(\boldsymbol{X}) = \begin{bmatrix} \mathrm{Div}_{\Gamma}\left(A_{11}, A_{12}, A_{13}\right) \\ \mathrm{Div}_{\Gamma}\left(A_{21}, A_{22}, A_{23}\right) \\ \mathrm{Div}_{\Gamma}\left(A_{31}, A_{32}, A_{33}\right) \end{bmatrix} =: \nabla^{\Gamma}_{\boldsymbol{X}} \cdot \mathbf{A}. \tag{5}$$

3.2 Mechanical quantities

With the displacement field $\boldsymbol{u}\left(\boldsymbol{X}\right)$ and $\boldsymbol{x} = \boldsymbol{X} + \boldsymbol{u}\left(\boldsymbol{X}\right)$, the *surface* deformation gradient $\mathbf{F}_{\Gamma}$ of the continuously embedded sub-structures is

$$\mathbf{F}_{\Gamma} = \nabla^{\Gamma,\mathrm{dir}}_{\boldsymbol{X}} \boldsymbol{x}\left(\boldsymbol{X}\right) = \mathbf{I} + \nabla^{\Gamma,\mathrm{dir}}_{\boldsymbol{X}} \boldsymbol{u}\left(\boldsymbol{X}\right). \tag{6}$$

Then, analogously to the bulk material, the following mechanical quantities result for a linear-elastic, homogeneous, and isotropic Saint Venant–Kirchhoff material of the embed-

ded sub-structures on the level sets:

$$\begin{aligned}
\text{Green-Lagrange strain tensor on } \Gamma^c_{\boldsymbol{X}}\text{:}\quad & \mathbf{E}^{\text{dir}}_\Gamma = 1/2 \cdot \left(\mathbf{F}^{\text{T}}_\Gamma \cdot \mathbf{F}_\Gamma - \mathbf{I}\right),\ \mathbf{E}^{\text{tang}}_\Gamma = \mathbf{P} \cdot \mathbf{E}^{\text{dir}}_\Gamma \cdot \mathbf{P}, \\
\text{second Piola-Kirchhoff stress tensor on } \Gamma^c_{\boldsymbol{X}}\text{:}\quad & \mathbf{S}_\Gamma = \lambda_\Gamma \cdot \text{trace}\left(\mathbf{E}^{\text{tang}}_\Gamma\right) \cdot \mathbf{P} + 2\mu_\Gamma \mathbf{E}^{\text{tang}}_\Gamma, \\
\text{Cauchy stress tensor on } \Gamma^c_{\boldsymbol{x}}\text{:}\quad & \boldsymbol{\sigma}_\Gamma = \frac{1}{\Lambda} \cdot \mathbf{F}_\Gamma \cdot \mathbf{S}_\Gamma \cdot \mathbf{F}^{\text{T}}_\Gamma, \\
\text{first Piola-Kirchhoff stress tensor:}\quad & \mathbf{K}_\Gamma = \mathbf{F}_\Gamma \cdot \mathbf{S}_\Gamma
\end{aligned}$$

where the two Lamé constants of the sub-structures are $\lambda_\Gamma = \frac{E \cdot \nu}{1-\nu^2}$, $\mu_\Gamma = \frac{E}{2(1+\nu)}$ for membranes, and $\lambda_\Gamma = 0$, $\mu_\Gamma = \frac{E}{2}$ for fibres, with Young's modulus E and Poisson's ratio ν of the sub-structures. $\Lambda = \frac{\|\nabla_{\boldsymbol{x}} \phi\|}{\|\nabla_{\boldsymbol{X}} \phi\|} \cdot \det \mathbf{F}_\Omega$ is a line stretch for fibres and an area stretch for membranes when undergoing the displacement.

4 Coupled mechanical model for the bulk material with embedded sub-structures

4.1 Boundary value problem in strong form

The combined equilibrium statement of the bulk material in $\Omega_{\boldsymbol{x}}$ with the continuously embedded sub-structures in $\Gamma^c_{\boldsymbol{x}}$ is in strong form over the deformed configuration:

$$\nabla_{\boldsymbol{x}} \cdot \boldsymbol{\sigma}_\Omega(\boldsymbol{x}) + \nabla^\Gamma_{\boldsymbol{x}} \cdot \boldsymbol{\sigma}_\Gamma(\boldsymbol{x}) = -\boldsymbol{b}(\boldsymbol{x}) \quad \forall \boldsymbol{x} \in \Omega_{\boldsymbol{x}} = \bigcup_c \Gamma^c_{\boldsymbol{x}}. \tag{7}$$

As usual in finite strain theory, this equilibrium with respect to the deformed configuration may also be stated equivalently purely based on quantities in the undeformed configuration as

$$\nabla_{\boldsymbol{X}} \cdot \boldsymbol{K}_\Omega(\boldsymbol{x}) + \nabla^\Gamma_{\boldsymbol{X}} \cdot \mathbf{K}_\Gamma(\boldsymbol{X}) = -\boldsymbol{B}(\boldsymbol{X}) \quad \forall \boldsymbol{X} \in \Omega_{\boldsymbol{X}} = \bigcup_c \Gamma^c_{\boldsymbol{X}}. \tag{8}$$

Note that the body forces $\boldsymbol{b}(\boldsymbol{x})$ and $\boldsymbol{B}(\boldsymbol{X})$ may be further split into contributions of the bulk material and the embedded sub-structures, i.e., $\boldsymbol{b}(\boldsymbol{x}) = \boldsymbol{b}_\Omega + \boldsymbol{b}_\Gamma$ and $\boldsymbol{B}(\boldsymbol{X}) = \boldsymbol{B}_\Omega + \boldsymbol{B}_\Gamma$, respectively. This may, for example, be useful to consider dead load individually. With the definitions of the Green-Lagrange strain tensors $\mathbf{E}_\Omega$ and $\mathbf{E}^{\text{tang}}_\Gamma$ and the second Piola-Kirchhoff stress tensors $\mathbf{S}_\Omega$ and $\mathbf{S}_\Gamma$ from above, one may now straightforwardly obtain the displacement-based BVP for the displacements $\boldsymbol{u}(\boldsymbol{X})$ in strong form.

4.2 Boundary value problem in weak form

For any FEM analysis, the BVP must be stated in a weak form. Therefore, Eq. (8) has to be multiplied with test functions $\boldsymbol{w}$, integrated over the domain $\Omega_{\boldsymbol{X}}$, and the divergence theorem has to be applied. This is done individually for the parts referring to the bulk material and the embedded sub-structures.

Then, for the bulk part, there follows:

$$\int_{\Omega_{\boldsymbol{X}}} \boldsymbol{w} \cdot (\nabla_{\boldsymbol{X}} \cdot \boldsymbol{K}_\Omega) \, \mathrm{d}\Omega = -\int_{\Omega_{\boldsymbol{X}}} \boldsymbol{w} \cdot \boldsymbol{B}_\Omega \, \mathrm{d}\Omega,$$
$$\int_{\Omega_{\boldsymbol{X}}} \nabla_{\boldsymbol{X}} \boldsymbol{w} : \mathbf{K}_\Omega \, \mathrm{d}\Omega = \int_{\Omega_{\boldsymbol{X}}} \boldsymbol{w} \cdot \boldsymbol{B}_\Omega \, \mathrm{d}\Omega + \int_{\partial\Omega_{\boldsymbol{X},\mathrm{N}}} \boldsymbol{w} \cdot \hat{\boldsymbol{H}}_\Omega \, \mathrm{d}\partial\Omega,$$

where $\hat{\boldsymbol{H}}_\Omega$ are tractions on the Neumann boundary $\partial\Omega_{\boldsymbol{X},\mathrm{N}}$ of the bulk material in the undeformed configuration.

For the embedded sub-structures, we integrate over the manifolds $\Gamma^c_{\boldsymbol{X}}$ within the level-set interval $(\phi^{\min}, \phi^{\max})$ and then use the so-called co-area formula [4, 6] to convert both of these integrals into *one* integral over $\Omega_{\boldsymbol{X}}$, which, for a scalar function $f(\boldsymbol{X})$ is

$$\int_{\phi^{\min}}^{\phi^{\max}} \int_{\Gamma^c_{\boldsymbol{X}}} f(\boldsymbol{X}) \, \mathrm{d}\Gamma \, \mathrm{d}c = \int_{\Omega_{\boldsymbol{X}}} f(\boldsymbol{X}) \cdot \|\nabla_{\boldsymbol{X}} \phi\| \, \mathrm{d}\Omega.$$

Hence, following previous works in [8, 7, 10], there holds

$$\int_{\phi^{\min}}^{\phi^{\max}} \int_{\Gamma^c_{\boldsymbol{X}}} \boldsymbol{w} \cdot \left(\nabla^\Gamma_{\boldsymbol{X}} \cdot \boldsymbol{K}_\Gamma\right) \mathrm{d}\Gamma \, \mathrm{d}c = -\int_{\phi^{\min}}^{\phi^{\max}} \int_{\Gamma^c_{\boldsymbol{X}}} \boldsymbol{w} \cdot \boldsymbol{B}_\Gamma \, \mathrm{d}\Gamma \, \mathrm{d}c,$$
$$\int_{\phi^{\min}}^{\phi^{\max}} \int_{\Gamma^c_{\boldsymbol{X}}} \nabla^{\Gamma,\mathrm{dir}}_{\boldsymbol{X}} \boldsymbol{w} : \mathbf{K}_\Gamma \, \mathrm{d}\Gamma \, \mathrm{d}c = \int_{\phi^{\min}}^{\phi^{\max}} \int_{\Gamma^c_{\boldsymbol{X}}} \boldsymbol{w} \cdot \boldsymbol{B}_\Gamma \, \mathrm{d}\Gamma \, \mathrm{d}c + \text{boundary term},$$
$$\int_{\Omega_{\boldsymbol{X}}} \left(\nabla^{\Gamma,\mathrm{dir}}_{\boldsymbol{X}} \boldsymbol{w} : \mathbf{K}_\Gamma\right) \cdot \|\nabla_{\boldsymbol{X}} \phi\| \, \mathrm{d}\Omega = \int_{\Omega_{\boldsymbol{X}}} (\boldsymbol{w} \cdot \boldsymbol{B}_\Gamma) \cdot \|\nabla_{\boldsymbol{X}} \phi\| \, \mathrm{d}\Omega + \text{boundary term}.$$

The boundary term vanishes under the assumption that, on the Neumann boundaries with respect to the embedded sub-structures, only zero-tractions $\hat{\boldsymbol{H}}_\Gamma = \boldsymbol{0}$ are considered.

Finally, we may state the combined weak form for the bulk material with embedded sub-structures as

$$\int_{\Omega_{\boldsymbol{X}}} \nabla_{\boldsymbol{X}} \boldsymbol{w} : \mathbf{K}_\Omega \, \mathrm{d}\Omega + \int_{\Omega_{\boldsymbol{X}}} \left(\nabla^{\Gamma,\mathrm{dir}}_{\boldsymbol{X}} \boldsymbol{w} : \mathbf{K}_\Gamma\right) \cdot \|\nabla_{\boldsymbol{X}} \phi\| \, \mathrm{d}\Omega$$
$$= \int_{\Omega_{\boldsymbol{X}}} \boldsymbol{w} \cdot (\boldsymbol{B}_\Omega + \boldsymbol{B}_\Gamma \cdot \|\nabla_{\boldsymbol{X}} \phi\|) \, \mathrm{d}\Omega + \int_{\partial\Omega_{\boldsymbol{X},\mathrm{N}}} \boldsymbol{w} \cdot \hat{\boldsymbol{H}}_\Omega \, \mathrm{d}\partial\Omega.$$

It is noted that only first-order derivatives are involved, allowing for the use of classical C_0-continuous finite elements in the corresponding *discrete* weak form. For the FEM-analyses presented in the numerical results below, the bulk domains $\Omega_{\boldsymbol{X}}$ are discretized with meshes composed of classical, possibly higher-order Lagrange elements. As seen in Fig. 2, these meshes do by no means have to align with the level sets in the bulk domain.

5 Numerical results

5.1 Test case in two dimensions with embedded fibres

The first test case was proposed in [8]. The bulk domain is a quarter annulus centered at the origin with an inner radius of $R_\mathrm{i} = 8$ and an outer radius of $R_\mathrm{o} = 12$, see Fig. 3(a).

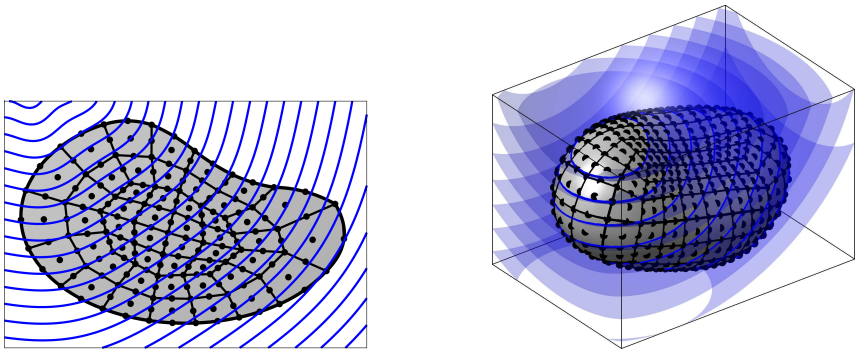

(a) $\Omega_{\boldsymbol{X}} \in \mathbb{R}^2$ (b) $\Omega_{\boldsymbol{X}} \in \mathbb{R}^3$

Figure 2: The bulk domains are discretized by d-dimensional, possibly higher-order elements which do not have to conform to the level sets.

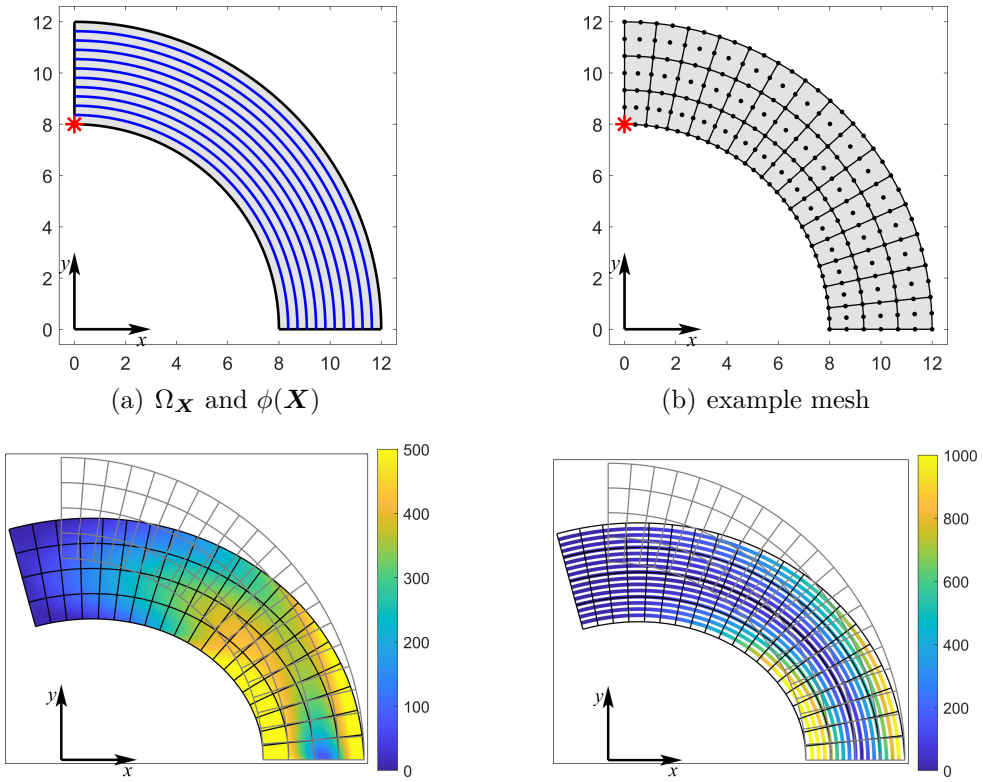

(a) $\Omega_{\boldsymbol{X}}$ and $\phi(\boldsymbol{X})$ (b) example mesh

(c) σ_{V} in $\Omega_{\boldsymbol{x}}$ (d) σ_{V} on $\Gamma^c_{\boldsymbol{x}}$

Figure 3: Test case with two-dimensional bulk domain and embedded fibres: (a) Undeformed bulk domain $\Omega_{\boldsymbol{X}}$ with selected level sets of $\phi(\boldsymbol{X})$, (b) example mesh for the FEM analysis, (c) von-Mises stresses σ_{V} in $\Omega_{\boldsymbol{x}}$ and (d) on selected level sets $\Gamma^c_{\boldsymbol{x}}$.

A set of fibres is implied via a level-set function $\phi(\boldsymbol{X}) = \|\boldsymbol{X}\| = \sqrt{X^2 + Y^2}$ in the level-set interval $(\phi^{\min},\ \phi^{\max}) = (R_{\mathrm{i}}, R_{\mathrm{o}})$. A Young's modulus of $E_\Omega = 10\,000$ and Poisson's ratio of $\nu_\Omega = 0.3$ are prescribed in the bulk domain and the Lamé constants λ_Ω and μ_Ω are computed according to plane strain conditions. For the fibres, we set $E_\Gamma = 19\,000$ and the cross-section $A = 1$ and compute λ_Γ and $\mu_\Gamma = 0$ accordingly. There is a body force of $\boldsymbol{B}_\Omega(\boldsymbol{X}) = [0, -20]^{\mathrm{T}}$ acting on the bulk material only (i.e., there are no additional body forces $\boldsymbol{B}_\Gamma$ on the fibres). As Dirichlet boundary conditions, zero-displacements, $\boldsymbol{u} = \boldsymbol{0}$, are prescribed on the lower side of the bulk domain where $Y = 0$.

An example mesh used in the finite element analysis is seen in Fig. 3(b), using quadratic Lagrange elements. We have systematically employed sequences of meshes with increasing numbers of elements and orders. The deformed domain is shown in Fig. 3(c) with the von-Mises stresses σ_{V} in the bulk material and in Fig. 3(d) with σ_{V} in the fibres. We observe a stored elastic energy in the bulk material of $\mathfrak{e}_\Omega(\boldsymbol{u}) = 336.684$ and in the fibres of $\mathfrak{e}_\Gamma(\boldsymbol{u}) = 337.6795$, resulting in a total energy of $\mathfrak{e}(\boldsymbol{u}) = 674.363$. Furthermore, the displacement of the lower left node, see the red marker in Figs. 3(a) and (b), is $\boldsymbol{u}(0, 8) = [-1.0194534, -2.710712]^{\mathrm{T}}$. For further details including a relation to discretely (rather than continuously) embedded fibres, see [8].

5.2 Test case in three dimensions with embedded membranes

The next test case is the first time where membranes are continuously embedded in a three-dimensional bulk material through the proposed approach. The bulk domain is a box in $[0, 3] \times [0, 0.2] \times [0, 0.2]$ as seen in Fig. 4(a). The set of embedded membranes is implied via a level-set function $\phi(\boldsymbol{X}) = \sqrt{Y^2 + Z^2} - 0.1$ in the level-set interval $(\phi^{\min},\ \phi^{\max}) = \left(0, \sqrt{2} \cdot 0.2\right) - 0.1$, see again Fig. 4(a) for some selected level sets. The geometric situation resembles an idealized timber beam. A Young's modulus of $E_\Omega = 5\,000$ and Poisson's ratio of $\nu_\Omega = 0.3$ are prescribed in the bulk domain and the Lamé constants λ_Ω and μ_Ω are computed accordingly. For the membranes, we set $E_\Gamma = 50\,000$ and the thickness $t = 1$ and compute λ_Γ and μ_Γ accordingly. There is a body force of $\boldsymbol{B}_\Omega(\boldsymbol{X}) = [0, 0, -5]^{\mathrm{T}}$ acting on the bulk material only (i.e., $\boldsymbol{B}_\Gamma = \boldsymbol{0}$ on the membranes). As Dirichlet boundary conditions, zero-displacements, $\boldsymbol{u} = \boldsymbol{0}$, are prescribed on the front side of the bulk domain where $X = 0$.

An example mesh used in the finite element analysis is seen in Fig. 4(b), using quadratic, hexahedral Lagrange elements and some mesh grading towards the support at $X = 0$. We are again systematically using sequences of meshes with increasing element numbers and orders. The deformed domain is shown in Fig. 4(c) with the von-Mises stresses σ_{V} in the bulk material and, in Fig. 4(d), with σ_{V} on some selected membranes (i.e., level sets). We observe a stored elastic energy in the bulk material of $\mathfrak{e}_\Omega(\boldsymbol{u}) = 0.004196$ and in the membranes of $\mathfrak{e}_\Gamma(\boldsymbol{u}) = 0.02996$, resulting in a total energy of $\mathfrak{e}(\boldsymbol{u}) = 0.03416$. Furthermore, the displacement of the back node as shown by the red marker in Figs. 4(a) and (b), is $\boldsymbol{u}(3, 0, 0) = [-0.02730, -0.00246, -0.28217]^{\mathrm{T}}$.

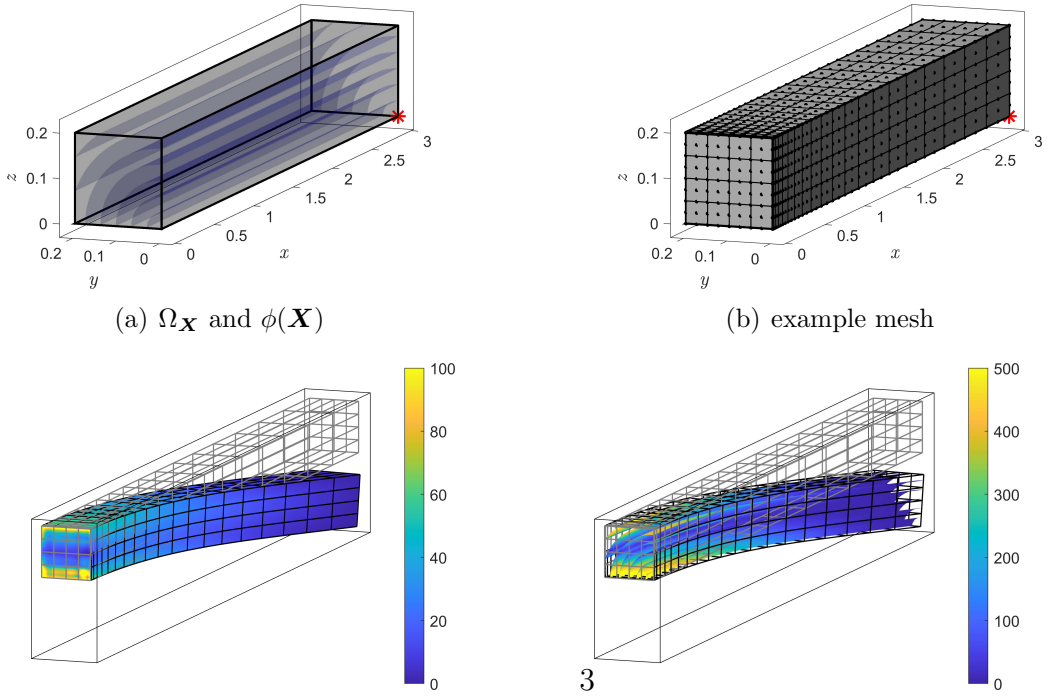

(a) $\Omega_{\boldsymbol{X}}$ and $\phi(\boldsymbol{X})$ (b) example mesh

(c) σ_{V} in $\Omega_{\boldsymbol{x}}$ (d) σ_{V} on $\Gamma^c_{\boldsymbol{x}}$

Figure 4: Test case with three-dimensional bulk domain and embedded membranes: (a) Undeformed bulk domain $\Omega_{\boldsymbol{X}}$ with selected level sets of $\phi(\boldsymbol{X})$, (b) example mesh for the FEM analysis, (c) von-Mises stresses σ_{V} in $\Omega_{\boldsymbol{x}}$ and (d) on selected level sets $\Gamma^c_{\boldsymbol{x}}$.

6 Conclusions

A strategy for continuously embedding $(d-1)$-dimensional sub-structures into d-dimensional bulk materials is proposed. For two-dimensional bulk domains, these sub-structures are (curved) fibres, for three-dimensional bulk domains, these are (curved) embedded membranes. The geometry of the sub-structures is implied by all level sets of a scalar function over the bulk domain. The mechanical model for the homogeneous and isotropic bulk material is given by classical finite strain theory. For the sub-structures, the tailored bulk models as proposed in [8, 10], are employed and coupled to the bulk material. The resulting *coupled* mechanical behaviour is naturally anisotropic, depending on the shapes of the embedded sub-structures. For the numerical analysis, higher-order elements in the bulk domain are used, with no need to align to the level sets. For the sub-structures, this is similar to the Bulk Trace FEM as proposed in [8, 10], however, herein coupled to a standard FEM treatment of the bulk material. The numerical results confirm the success of the new formulation. The next step is to also include *fibres* in *three*-dimensional bulk domains. Then, each fibre family is implied by two level-sets and proper mechanical models have to be derived. We see large potential for embedding sub-structures in bulk materials, e.g., in advanced material models, possibly labeled *continuously embedded sub-structure models* with possible applications, e.g., in textile, biomechanical or fibre-reinforced structures and composite laminates.

REFERENCES

[1] Adalsteinsson, D.; Sethian, J.A.: Transport and diffusion of material quantities on propagating interfaces via level set methods. *J. Comput. Phys.*, **185**, 271–288, 2003.

[2] Delfour, M.C.; Zolésio, J.P.: *Shapes and geometries—Metrics, Analysis, Differential Calculus, and Optimization.* SIAM, Philadelphia, PA, 2011.

[3] Dziuk, G.; Elliott, C.M.: An Eulerian approach to transport and diffusion on evolving implicit surfaces. *Comput. Vis. Sci.*, **13**, 17–28, 2008.

[4] Dziuk, G.; Elliott, C.M.: Eulerian finite element method for parabolic PDEs on implicit surfaces. *Interfaces and Free Boundaries*, **10**, 2008.

[5] Dziuk, G.; Elliott, C.M.: An Eulerian approach to transport and diffusion on evolving implicit surfaces. *Computing and Visualization in Science*, **13**, 17–28, 2010.

[6] Federer, H.: *Geometric measure theory.* Springer, New York, 1969.

[7] Fries, T.P.; Kaiser, M.W.: The Bulk Trace FEM for the Simultaneous Solution of Structural Membranes on all Level-sets over a Bulk Domain. *Proceedings in Applied Mathematics and Mechanics*, Vol. 23, John Wiley & Sons, Chichester, 2023.

[8] Fries, T.P.; Kaiser, M.W.: On the Simultaneous Solution of Structural Membranes on all Level Sets within a Bulk Domain. *Comp. Methods Appl. Mech. Engrg.*, **415**, 116223, 2023.

[9] Fries, T.P.; Schöllhammer, D.: A unified finite strain theory for membranes and ropes. *Comp. Methods Appl. Mech. Engrg.*, **365**, 113031, 2020.

[10] Kaiser, M.W.; Fries, T.P.: Simultaneous solution of ropes and membranes on all level sets within a bulk domain. *Proceedings in Applied Mathematics and Mechanics*, Vol. 23, John Wiley & Sons, Chichester, 2023.

[11] Kaiser, M.W.; Fries, T.P.: Simultaneous analysis of continuously embedded Reissner-Mindlin shells in 3D bulk domains. *Internat. J. Numer. Methods Engrg.*, **e7495**, 0–0, 2024.

[12] Osher, S.; Fedkiw, R.P.: *Level Set Methods and Dynamic Implicit Surfaces*. Springer, Berlin, 2003.

[13] Schöllhammer, D.; Fries, T.P.: Kirchhoff-Love shell theory based on Tangential Differential Calculus. *Proceedings in Applied Mathematics and Mechanics*, Vol. 18, John Wiley & Sons, Chichester, 2018.

[14] Schöllhammer, D.; Fries, T.P.: Reissner-Mindlin shell theory based on tangential differential calculus. *Comp. Methods Appl. Mech. Engrg.*, **352**, 172–188, 2019.

[15] Schöllhammer, D.; Fries, T.P.: A unified approach for shell analysis on explicitly and implicitly defined surfaces. In *Proceedings of the IASS Annual Symposium 2019 (Form and Force, Structural Membranes 2019)*. (Lázaro, C.; Bletzinger, K.U.; Oñate, E.; Oñate, E., Eds.), Barcelona, Spain, 750–757, 2019.

[16] Schöllhammer, D.; Fries, T.P.: A higher-order Trace finite element method for shells. *Internat. J. Numer. Methods Engrg.*, **122**, 1217–1238, 2021.